Zhang, C., Shen, C., Yang, Y. Y., Dunlop, M. W., Russell, T. C., Lühr, H., Burch, J. L., Lindquist, P. A., Torbert, R. B., Friis-Christensen, E. (2019): Near-Earth vortices' driving of field-aligned currents: Magnetospheric Multi-Scale and Swarm observations. - *Chinese Journal of Space Science*, *39*, 1, pp. 9—17.

DOI: http://doi.org/10.11728/cjss2019.01.09

Near-Earth Vortices' Driving of Field-Aligned Currents: Magnetospheric Multiscale and Swarm Observations*

C ZHANG[1,2] C SHEN[3] Y Y YANG[4] M W DUNLOP[5,6] S TI[1,2]

C T RUSSELL[7] HLÜHR[8] J L BURCH[9] P A LINDQVIST[10]

R B TORBERT[11] FRIIS-CHRISTENSEN[12]

1（*State Key Laboratory of Space Weather, National Space Science Center, Beijing* 100190）

2（*College of Earth Science, University of Chinese Academy of Sciences, Beijing* 100049）

3（*College of Science, Harbin Institute of Technology* (*Shenzhen*), *Shenzhen* 518055）

4（*Institute of China Seismological Bureau*, *Crustal Stress*, *Beijing* 100085）

5（*Space Science Institute*, *School of Astronautics*, *Beihang University*, *Beijing* 100191）

6（*Rutherford Appleton Laboratory*, *Didcot OX*11 *0QX*）

7（*University of California*, *Los Angeles*, *California CA*90024）

8（*GFZ*, *German Research Center for Geosciences*, *Potsdam D*-14473）

9（*Southwest Research Institute*, *San Antonio*, *Texas TX*78238）

10（*Royal Institute of Technology*, *Stockholm S*-10044）

11（*University of New Hampshire*, *Durham*, *New Hampshire NH*03824）

12（*Danish National Space Center*, *Copenhagen DK*-2100）

*Supported by National Natural Science Foundation of China(41874190,41231066)
Received November 30, 2017. Revised June 22, 2018
E-mail: shenchao@hit.edu.cn

AbstractA long-standing mystery in the study of Field-Aligned Currents (FACs) has been that: how the currents are generated and why they appear to be much stronger at high altitudes than in the ionosphere. Here we present two events of magnetotail FACs observed by the Magnetospheric Multiscale Spacecraft (MMS) on 1st July and 14th July 2016, to show how the Substorm Current Wedges (SCW) were formed. The results show that particles were transferred heading towards the Earth during the expansion phase of substorms. The azimuthal flow formed clockwise (counter-clockwise) vortex-like motion, and then generated downward (upward) FACs on the tailward/poleward side of the distorted field with opposite vorticity on their earthward/equatorward side. We also analyzed the Region 1 FACs observed by the Earth Explorer Swarm spacecraft on 1st July 2016 and found that they were associated with FACs observed by MMS, although differing by a factor of 10. This difference suggests that either there was the closure of the currents at altitudes above 500km or the currents were not strictly parallel to B and closed at longitudes away from where they were generated.

Keywords: Substorm current wedge, Magnetosphere, Field-aligned currents, Flow vorticity, Multiple spacecraft measurements

0 Introduction

Field-Aligned Currents (FACs), first suggested by *Birkeland* [1], are believed to be the keyways by which momentum and energy can be transferred between the magnetosphere and the ionosphere [2-4]. FACs between the magnetosphere and the ionosphere exist continuously and are strictly conserved, which provides a unique opportunity to gain insight into the underlying physical processes in the magnetosphere [5]. These currents play an important role: In the region near noon, they link to the polar ionosphere directly along open field lines, while they link to the plasma sheet at most other longitudes [6].

Chun and *Russell* [7] have studied the occurrence rate related to geomagnetic activity in the inner magnetosphere, finding that, when auroral activity is strong ($|AL| > 135$nT), magnetospheric internal stresses become much greater, and leading to the widespread occurrence of FACs in the Earth's inner magnetosphere. FACs in the magnetosphere show as much range as currents in the auroral ionosphere and vary in concert with these currents too. However, the origin of FACs is still an open issue.

In the magnetotail, FACs is the vertical part of the SCW, and its association with FAC is an essential feature of substorm expansion. From the momentum equation for isotropic pressure, two source terms for the SCW generation have been suggested; they are the inertial currents and the pressure gradient currents,

$$\nabla \cdot \mathbf{j}_{\parallel} = -\nabla \cdot \mathbf{j}_{\perp} = -\nabla \cdot \left(\frac{\mathbf{B}}{B^2} \times \rho \frac{d\mathbf{u}}{dt} + \frac{\mathbf{B}}{B^2} \times \nabla P \right). \tag{1}$$

The first term on the right-hand side in (1) represents the inertial currents and the second is the diamagnetic currents. It is generally believed that the inertial currents are more relevant to the generation of FACs in the substorms initial dynamic phase [8,9]. Alternatively, resulting from the change of vorticity (Ω) and the magnetic field, a direct expression for the FACs can be derived [10] as

$$j_{\parallel} = B_i \int_{eq}^{ion} \frac{\rho}{B} \frac{d}{dt} \left(\frac{\Omega}{B} \right) dl_{\parallel}, \tag{2}$$

Where ρ is the mass density and $\Omega = \mathbf{B} \cdot \nabla \times \mathbf{V}/B$, which refers to the field-aligned component of vorticity. *Hasegawa* and *Sato* [10] and *Vasyliunas* [11] have suggested that the time-increasing vorticity can produce FACs during magnetospheric substorms. *Haerendel* [8] has proposed that a dawnward inertia current will be caused at the stopping point when the flows are slow down. *Keiling et al.* [12] have showed that a clockwise (counterclockwise) magnetospheric vortex-like motion corresponds to downward (upward) FACs and the related part in Eq.(3) contributes a significant part or all of the FACs of the SCW at onset of the substorm expansion phase, although would be later replaced by some other generating mechanisms such as the pressure gradient [13-17]. *Shi* et al. [18] have reported in situ and ground observations of a solar wind dynamic pressure enhancement induced vortex in the nightside plasma sheet and carried out magnetohydrodynamics simulations. Based on both observation and simulation technique, *Tian* et al. [19] have shown that the main impulse related FACs are correlated with the large-scale flow vortex in the dayside magnetosphere, *Zhao* et al.[20] have reported a vortex's formation and propagation down the magnetotail after solar wind dynamic pressure decrease. Besides, most of the substorm models take the formation of flow vorticity and associated FAC generation into consideration, and numerical simulations also allow for the vortex mechanism operating in the magnetotail.

Since the first identification of FACs, a vast number of studies have been reported, among them, most are based on single-spacecraft or surface observations[21,22] However, FACs have seldom been directly spatially measured, although their physical characteristics have been extensively studied[23,24], especially during substorms, FACs would be more complicated near the night side. One way to solve these problems at higher magnetospheric distances is using multi-spacecraft analysis [25,26].

In this paper, we report FACs observations using the MMS spacecraft [27] and the Swarm [28] satellite. We calculate the magnetotail current density and vorticity at the MMS center using Magnetic Rotation Analysis (MRA) [29,30]. By analyzing and contrasting the characteristics of R1 type FACs, magnetotail FACs, and vortex motions, we investigate the origin and evolution of FACs. Geocentric Solar Magnetic (GSM) coordinates system is used throughout this study expect special remarks.

1 Case Studies

In this section, two moderate substorm events will be investigated using measurements from four MMS satellites that were near the equatorial plane in a tetrahedral configuration. Figure 1(a) and 1(b) show their projected locations on the X-Y plane. During both substorm events, the four MMS satellites were located near the midnight region, at ~11 R_E (where R_E is the Earth radius, 6371km) tailward from

Earth. Figure 1(c) shows variations of *AE* and *AL* indexes from 07:00 to 10:00 UT on 01 July 2016, and the Magnetic Local Time (MLT) interval is from 23.27 to 23.83. Both *AE* and *AL* indexes varied dramatically at 08:24 UT, which indicates the beginning of the expansion phase. The *AE* index reached a maximum value of 681nT while the *AL* index reached a minimum value of −479nT at 08:56 UT, then these two indices declined. Figure 1(d) shows the evolution of the second substorm event from 05:00 to 08:00 UT on 14 July 2016, and the MLT interval is 22.40 to 23.00. The maximum value of the *AE* index is 1003nT and the minimum value of the *AL* index is −709nT.

Figure 2(a) shows the magnetic field disturbance observed by the MMS1 spacecraft during 08:30 to 09:00 UT on 01 July 2016, the data are from the fluxgate magnetometer [31], and Figure 2(b) shows the magnetic field disturbance during the other event. Owing to the small distance separating the four MMS satellites, the magnetic field of each component and the total value are almost identical in size and trends in four satellites.

The four MMS spacecraft were launched on 12 March 2015 to explore the microphysics of magnetic reconnection. They travel in two highly elliptical Earth orbits. Each orbit is designed to pass through two separate areas of magnetic reconnection in near-Earth space. During mission operations, the MMS spacecraft form adjustable tetrahedral configurations, and their instruments can yield scientific data of unprecedented high precision and resolution.

The three Swarm spacecraft were launched on 22 November 2013 and placed into circular, low-Earth polar orbits since the start of science operations on 17 April 2014. The Swarm B flies at a relatively drifting orbit, at a mean high-latitude altitude of ~531km, with an orbital period of ~95 minutes. The Swarm mission provides the first global dataset representation of geomagnetic field variations on time scales from an hour to several years.

2.1. Case 1

In Figures 3(a), we depict the magnetotail current density in the local natural coordinates at the center of the MMS tetrahedron from 08:43 to 08:49 UT obtained via the MRA techniques, the red line represents the field-aligned component. The maximum value of current density is about $40\mathrm{nA/m^2}$ in the yellow shaded portion (from 08:45:50 to 08:46:50 UT), the currents flaw down toward the Earth, the shaded region represents the time corresponding to Earthward plasma flow. In Figure 3b, we estimated the current density in unit magnetic flux, using the formula $\boldsymbol{J} = j/B$, in units of $\mathrm{A \cdot W^{-1}}$, the value increased up to ~$1\mathrm{A \cdot W^{-1}}$ at 08:46:23 UT.

This observational event occurred in the first stage of MMS operations, during which some instruments were not working during magnetotail crossing, thus particle data were not available. On this account, we infer the flow from electric drift measurements, using the slow-flow approximation plasma drift results from electric drift: $\mathbf{V}_E = \mathbf{E} \times \mathbf{B}/B^2$[32-33]. The DC-coupled electric field data are from the Electric Double Probes (EDP)[34-36]. Figure 3(c)~(e) show the electric drift velocity calculated by using the magnetic and electric fields. The speed shear was existed in the Y direction throughout the observation, however did not in in the X and Z directions, *Kepko et al.* [37] suggested that the speed shear on the both dusk and morning sides is the primary source of the currents driving the substorm current wedge. It is now well established that the onset of the substorms expansion phase is associated with plasma sheet flow velocity [38-40]. In this event, all three velocity components increased rapidly by 08:46:00 UT, the V_X rose to 200km/s, the value of V_Y increased up to 600km/s, andV_Z increased to 300km/s, which indicated energetic particles flaw toward the Earth, and then the components decreased to near zero at 08:46:15 UT, and then appeared vortex motion.

Base on *Keiling et al*., [12] and *Lui et al*., [41],

$$j_{\|} \approx 2 \cdot \left(\frac{n m_H}{B_{eq.avg}}\right)\left(\frac{v_{final}}{\tau}\right)\left(\frac{L}{r}\right), \tag{3}$$

Where $B_{eq.avg}$ is the value of the equatorial magnetic field averaged over the four satellites, v_{final} is the rotational vortex speed averaged over the four spacecraft, τ is the time scale of the vorticity change, L is the plasma sheet thickness and r is the scale of the vortex. Using $\mathrm{n} \approx 1 \cdot \mathrm{cm}^{-3}$, $B_{eq.avg} \approx 40\mathrm{nT}$,$v_{final}$ ≈$700\mathrm{km} \cdot \mathrm{s}^{-1}$, $\tau = 40\mathrm{s}$, $\mathrm{L} = 1\mathrm{R_E}$ and $\mathrm{r} = 1\mathrm{R_E}$, we obtained a downward current density in the equatorial region of approximately $1.47\mathrm{nA} \cdot \mathrm{m}^{-2}$, which is much smaller than the measured data. The above calculation used the assumption of a solid-body rotation for the vortex, however, we found pulsed vorticity existed in the event. Figure 3(f) shows the value of vorticity calculated via the MRA in the local natural coordinates, several transient vortices formed during the period. The tendency of vorticity along field-aligned direction (Ω_B) had a correspondence to the FACs and in opposite direction. At 08:46:15 UT, the value of Ω_B increased to $27\mathrm{s}^{-1}$ when particle speed descended. We assumed that the individual vortex each generate a small current wedge, and collectively cause a downward/upward FACs, which should be a much more complicated system.

2.2. Case 2

Figures 4 is an overview of current density, electric drift velocity and vorticity in the same format as in Figure 3, the yellow shaded portion period is from 06:06:30 to 06:11:30 UT. During the period, the maximum value of current density is about $30\mathrm{nA}\cdot\mathrm{m}^{-2}$, and the maximum magnitude of current density in unit magnetic flux is ~$1\mathrm{A}\cdot\mathrm{W}^{-1}$. Again, we used electric drift velocity, what is different from the former is all three components existed speed shear. During the yellow shaded period, we distinguished 5 main Earthward flows, and the maximal downward current density we obtained was approximately $4.24\mathrm{nA}\cdot\mathrm{m}^{-2}$ using the assumption of a solid-body rotation, we did notice that the boosting of the FACs along with the pulsed vorticities emerging, and the maximum value of Ω_B is about 25 s^{-1}.

2.3. Swarm observation

Figure 5(c) is the current density of R1 type FACs variation during the substorm interval on 01 July 2016 observed by Swarm B, and the maximum value is about $4.3\mu\mathrm{A}\cdot\mathrm{m}^{-2}$ at 02.75 MLT, 14 seconds after the peak value of magnetotail FACs in Figure 5(a). Figure 5(d) shows the R1 type current density in unit flux, and the number increased to $0.1\mathrm{A}\cdot\mathrm{W_b}^{-1}$ at 08:46:37 UT. Both currents were flowed into the ionosphere and existed an association, but differ by a factor of 10. Assume the R1 type FACs are range from $4\mu A \cdot m^{-2}$ to $20\mu A \cdot m^{-2}$, which have an average value of $\sim 2.2\,\mu A \cdot m^{-2}$ [42,43], and the current density in unit magnetic flux is $0.1\sim 0.4 A \cdot W_b{}^{-1}$. From the perspective of value, magnetotail FACs are enough to drive R1 type FACs.

The MMS and Swarm satellites are independent detection plans and serve for different scientific objectives, so it is difficult for them to have perfect cooperation in the joint observation. In this substorm event, the MMS and Swarm satellites were not exactly in the same magnetic flux tube, although their magnetic local time and latitude were close. We believe that FACs in the magnetotail and polar regions are coupled in the event, but the timing issue of a substorm on the minute scale could not be analyzed and is not the purpose of this work. However, the generation mechanism of substorm can be our future research, and we hope to find better observation events.

2 Summary and Discussion

In this paper, by analyzing two medium substorm events, we investigated and analyzed the characteristics of FACs, obtaining some new clues. We calculated the magnetotail current density and current density in unit magnetic flux at the center of four MMS satellites via MRA. In addition, to study the relationship between FACs and vortex flow, we computed the vorticity.

Downward (upward) FACs in the magnetotail produced at the stopping point, after particle speed increased rapidly. For case 1, a main process of particle speed ascending and then descending is observed, the maximum of the current density at the center of MMS is about $40\mathrm{nA}\cdot\mathrm{m}^{-2}$, and the current density in unit magnetic flux is ~$1\mathrm{A}\cdot\mathrm{W}^{-1}$. The maximum value for case 2 is about $25\mathrm{nA}\cdot\mathrm{m}^{-2}$, and ~$1\mathrm{A}\cdot\mathrm{W}^{-1}$ with several velocity ascending and descending processes. For both cases, the maximum value of Ω_B is about $25\mathrm{s}^{-1}$. Multiple individual clockwise (counter-clockwise) flow vortex is observed in the substorm expansion phase, associated with the intensifying of current density. The Ω_B has a pulsed uplift at some moments, means some transient vortex are formed in the equatorial plane, and has an opposite direction to the magnetotail FACs, which means clockwise vortex corresponds to downward FACs, and vice versa. We assumed that each vortex can generate a small current wedge, and collectively cause a downward/upward FACs.

For the first substorm event, the R1 type FACs are also studied, the current with a maximum value of $4.3\mu\mathrm{A}\cdot\mathrm{m}^{-2}$ and $0.1\mathrm{A}\cdot\mathrm{W}^{-1}$, and had an association with the magnetotail FACs. It is noteworthy that the event is moderate with the peak of theAE index reaching 681nT.

The generation mechanism of the SCW is an unsolved mystery, we have found that pulsed vortex is relevant, so quantifying the contribution of a pulsed vortex to the FACs will be the topic in our future studies.

Acknowledgments. The study is partly supported through the ISSI Teams. We thank the World Data Center for Geomagnetism, Kyoto, the ESA Swarm project, and the MMS Science Data Center for providing the data used here. AE index data were obtained from http://wdc.kugi.kyoto-u.ac.jp/index.html. MMS data were obtained from ftp://cdaweb.gsfc.nasa.gov/pub/data/mms/, and Swarm data were acquired from

ftp://swarm-diss.eo.esa.int/.

References

[1] BIRKELAND K., The Norwegian Aurora Polaris Expedition 1902–1903\,[M], sect. 1, Aschhoug, Oslo, 1908.

[2] FOSTER J. C., ST.-MAURICEJ P, ABREU V. J.(1983) Joule heating at high latitudes\,[J], {\it J. Geophys. Res.}, {\bf 88}(A6):\,4885–4896, DOI:10.1029/JA088iA06p04885.

[3] LUIA. T. Y. (1996), Current disruption in the Earth's magnetosphere: Observations and models\,[J], {\it J. Geophys. Res.}, {\bf 101}(A6):\,13067-13088, DOI:10.1029/96JA00079.

[4] LU G., BAKER D. N., MCPHERRON R. L., {\it et al.} (1998), Global energy deposition during the January 1997 magnetic cloud event\,[J], {\it J. Geophys. Res.}, {\bf 103}(A6):\,11685–11694, DOI: 10.1029/98JA00897.

[5] IIJIMA T (2000), Field-aligned currents in geospace: Substance and significance\,[M].

[6] STERN D. P (1983), The origins of Birkeland currents\,[J]. {\it Rev. Geophys.}, {\bf 21}(1):\,125-138, DOI:10.1029/RG021i001p00125.

[7] CHUN F. K., and RUSSELL C. T. (1997), Field-aligned currents in the inner magnetosphere: Control by geomagnetic activity\,[J]. {\it J. Geophys. Res.}, {\bf 102(A2)}:\,2261-2270, DOI: 10.1029/96JA01819.

[8] HAERENDELG (1992), Disruption, ballooning or auroral avalanche-On the cause of substorms, in Proceedings of the International Conference on Substorms (ICS-1).

Eur. Space Agency Spec. Publ., ESA SP-335, 417–420.

[9] SHIOKAWA K., BAUMJOHANN W., and HAERENDEL G. (1997), Braking of high-speed flows in the near-Earth tail\,[J]. {\it Geophys. Res. Lett.}, 24(10), 1179–1182, DOI:10.1029/97GL01062.

[10] HASEGAWA A., and SATOT. (1979), Generation of field aligned current during substorm\,[J], {\it in Dynamics of the Magnetosphere}. edited by S.-I. Akasofu, pp. 529–542, DOI:10.1007/978-94-009-9519-2_28.

[11] VASYLIUNAS V. M (1984), Fundamentals of current description, in Magnetospheric Currents\,[J]. {\it Geophys. Monogr.Ser.}, vol. {\bf 28}.

[12] KEILING A., ANGELOPOULOS V., RUNOV A.,{\it et al. }(2009), Substorm current wedge driven by plasma flow vortices: THEMIS observations\,[J]. {\it J. Geophys. Res.}, {\bf 114(A1)}:A00C22, DOI:10.1029/2009JA014114.

[13] BIRN J., HESSEM., HAERENDELG., {\it et al.}(1999), Flow braking and the substorm current wedge\,[J], {\it J. Geophys. Res.}, {\bf 104}(A9):\,19895–19903, DOI:10.1029/1999JA900173.

[14] BIRN J., RAEDER J.,WANG Y. L., {\it et al.} (2004), On the propagation of bubbles in the geomagnetic tail\,[J], {\it Ann. Geophys.}, {\bf 22}, 1773–1786, DOI: 10.5194/angeo-22-1773-2004.

[15] WANG C., SUN T. R., GUO X. C., {\it et al.} (2010), Case study of nightsidemagnetospheric magnetic field response to interplanetary shocks\,[J], {\it J. Geophys. Res.}, {\bf 115}(A10):, DOI:10.1029/2010JA015451.

[16] XING X., LYONS L. R., NISHIMURAY., {\it et al.} (2011), Near-Earth plasma

sheet azimuthal pressure gradient and associated auroral development soon before substorm onset\,[J], {\it J. Geophys. Res.}, {\bf 116}(A7), DOI:10.1029/2011JA016539.

[17] YAO Z. H., PU Z. Y., FU S. Y.,{\it et al.}, (2012), Mechanism of substorm current wedge formation: THEMIS observations\,[J], {\it Geophys. Res. Lett.}, VOL. {\bf 39}(13), DOI:10.1029/2012GL052055.

[18] SHI Q.Q., HARTINGER M.D., ANGELOPOULOS V., {\it et al.} (2014), Solar wind pressure pulse-driven magnetospheric verticesand their global consequences\,[J], {\it J. Geophys. Res. Space Physics}, 119(6), 4274–4280, DOI:10.1002/2013JA019551.

[19] TIAN A. M., SHEN X. C., SHI Q. Q., {\it et al. }(2016), Dayside magnetospheric and ionospheric responses to solar wind pressure increase: Multispacecraft and ground observations\,[J], {\it J. Geophys. Res. Space Physics}, {\bf 121}(11):\,10,813–10,830, DOI:10.1002/2016JA022459.

[20] ZHAO H. Y., SHEN X. C., TANG B. B., {\it et al.} (2016), Magnetospheric vortices and their global effect after a solar wind dynamic pressure decrease\,[J], {\it J. Geophys. Res. Space Physics}, {\bf 121(2)}:\,1071–1077, DOI:10.1002/2015JA021646.

[21] ZMUDA A. J., MARTIN J. H., and HEURING F. T. (1966), Transverse magnetic disturbances at 1100 kilometers in the auroral region\,[J], {\it J. Geophys. Res.}, {\bf 71}(21):\,5033–5045, DOI:10.1029/JZ071i021p05033.

[22] ZMUDA A. J., HEURING F. T., and MARTIN J. H. (1967), Dayside magnetic

disturbances at 1100 kilometers in the auroral oval\,[J], {\it J. Geophys. Res.}, {\bf 72}(3):\,1115–1117, DOI:10.1029/JZ072i003p01115.

[23] SHIOKAWA, K., BAUMJOHANN W., HAERENDEL G., {\it et al.}(1998), High-speed ion flow, substorm current wedge, and multiple Pi2 pulsations.{\it J. Geophys. Res.}, {\bf 103}(A3):\,4491–4507, DOI:10.1029/97JA01680.

[24] CAO J.B., YAN Chunxiao, DUNLOP Malcolm,{\it et al.} (2010), Geomagnetic signatures of current wedge produced by fast flows in a plasma sheet\,[J]. {\it J. Geophys. Res.}, {\bf 115(A8)}:A08205, DOI:10.1029/2009JA014891.

[25] SLAVIN J. A.,LE G., STRANGEWAY R. J., {\it et al.} (2008), Space technology 5 multi-point measurements of near-Earth magnetic fields: Initial results\,[J]. {\it Geophys. Res. Lett.}, {\bf 35(2)}:L02107, DOI:10.1029/2007GL031728.

[26] MARCHAUDON A., CERISIER J.C., DUNLOP M. W,{\it et al.} (2009), Shape, size, velocity and field-aligned currents of dayside plasma injections: A multi-altitude study\,[J]. {\it Ann. Geophys.}, {\bf 27}, 1251–1266, DOI:10.5194/angeo-27-1251-2009.

[27] BURCH J. L., MOORET. E., TORBERTR. B., {\it et al.} (2015), Magnetospheric multiscale overview and science objectives\,[J], {\it Space Sci. Rev.}, {\bf 199}（1-4）:\,5–21, DOI:10.1007/s11214-015-0164-9.

[28] FRIIS-CHRISTENSEN E., LÜHR H., KNUDSEN D., {\it et al.}(2008), Swarm -An Earth observation mission investigating Geospace\,[J]. {\it Adv}. {\it Space}{\it Res}.,{\bf 41}(1): 210–216, DOI:10.1016/j.asr.2006.10.008.

[29] SHEN C., LI X., DUNLOP M., {\it et al.} (2003), Analyses on the geometrical structure of magnetic field in the current sheet based on cluster measurements\,[J]. {\it J. Geophys. Res.}, {\bf 108}(A5):\,1168, DOI:10.1029/2002JA009612.

[30] SHEN C., LI X., DUNLOP M., {\it et al.} (2007), Magnetic field rotation analysis and the applications\,[J], {\it J. Geophys. Res.}, {\bf 112}(A6), A06211, DOI:10.1029/2005JA011584.

[31] RUSSELL C. T., ANDERSON B. J., BAUMJOHANN W.,{\it et al.} (2016), The Magnetospheric Multiscale Magnetometers\,[J], {\it Space Sci. Rev.}, {\bf 199}(1-4), 189–256, DOI:10.1007/s11214-014-0057-3.

[32] BOROVSKY J. E. and BONNELL. J (2001), The dc electrical coupling of flow vortices and flow channels in the magnetosphere to the resistive ionosphere\,[J], {\it J. Geophys. Res.}, {\bf 106}(A12):\,28967-28994, DOI: 10.1029/1999JA000245.

[33] WANG C.P., LYONS L. R., WOLF R. A., {\it et al.} (2009), Plasma sheet Pv$^{\{\backslash it\ 5/3\}}$ and nv and associated plasma and energy transport for different convection strengths and AE levels\,[J], {\it J. Geophys. Res.}, {\bf 114}(A9), A00D02, DOI:10.1029/2008JA013849.

[34] TORBERT R. B., RUSSELL C. T., MAGNES W., {\it et al.} (2016), The FIELDS Instrument Suite on MMS: Scientific Objectives, Measurements, and Data Products\,[J], {\it Space Sci. Rev.}, {\bf 199}(1-4):\,105-135, DOI:10.1007/s11214-014-0109-8.

[35] ERGUN R. E., TUCKER S., WESTFALL J., {\it et al.} (2016), The Axial Double Probe and Fields Signal Processing for the MMS Mission\,[J], {\it Space Sci.

Rev.}, {\bf 199}(1-4):\,167–188, DOI:10.1007/s11214-014-0115-x.

[36]LINDQVIST P.-A., OLSSON G., TORBERT R. B.,{\it et al.} (2016), The Spin-Plane Double Probe Electric Field Instrument for MMS\,[J], {\it Space Sci. Rev.}, {\bf 199(1-4)}:\,137–165, DOI:10.1007/s11214-014-0116-9.

[37] KEPKO L., MCPHERRON R.L., AMMO. {\it et al.}, (2015), Substorm Current Wedge Revisited\,[J]. {\it Space Sci. Rev.}{\bf 190}(1-4):\,1-46, DOI:10.1007/s11214-014-0124-9.

[38] HONES Jr. E. W., ASBRIDGE J. R., BAME S. J.,{\it et al.}(1973), Magnetotail plasma flow measured by Vela 4A\,[J], {\it J. Geophys. Res.}, {\bf 78}(25):\,5463–5476, DOI:10.1029/JA078i025p05463.

[39] MIYASHITA, Y., MACHIDA S., KAMIDE Y., {\it et al.} (2009), A state-of-the-art picture of substorm-associated evolution of the near-Earth magnetotail obtained from superposed epoch analysis\,[J], {\it J. Geophys. Res.}, 114(A1), DOI:10.1029/2008JA013225.

[40] MCPHERRON, R.L., HSU T.S., KISSINGER J., {\it et al.} (2011), Characteristics of plasma flows at the inner edge of the plasma sheet\,[J]. {\it J. Geophys. Res}.{\bf 116}(A5). DOI:10.1029/2010JA015923.

[41] LUI A. T. Y., SPANSWICK E., DONOVAN E. F.,{\it et al.} (2010), A transient narrow poleward extrusion from the diffuse aurora and the concurrent magnetotail activity\,[J], {\it J. Geophys. Res.}, {\bf 115}(A10), DOI:10.1029/2010JA015449.

[42] Iijima T, Potemra T A (1976), The amplitude distribution of field-aligned currents at northern high latitudes observed by Triad. J. Geophys. Res., 81, 2165-2174,

doi: 10.1029/JA081i013p02165.

[43] Iijima, T., and T. A. Potemra (1978), Large-scale characteristics of field-aligned currents associated with substorms. J. Geophys. Res., 83, 599-615, doi: 10.1029/JA083iA02p00599.

Figure captions

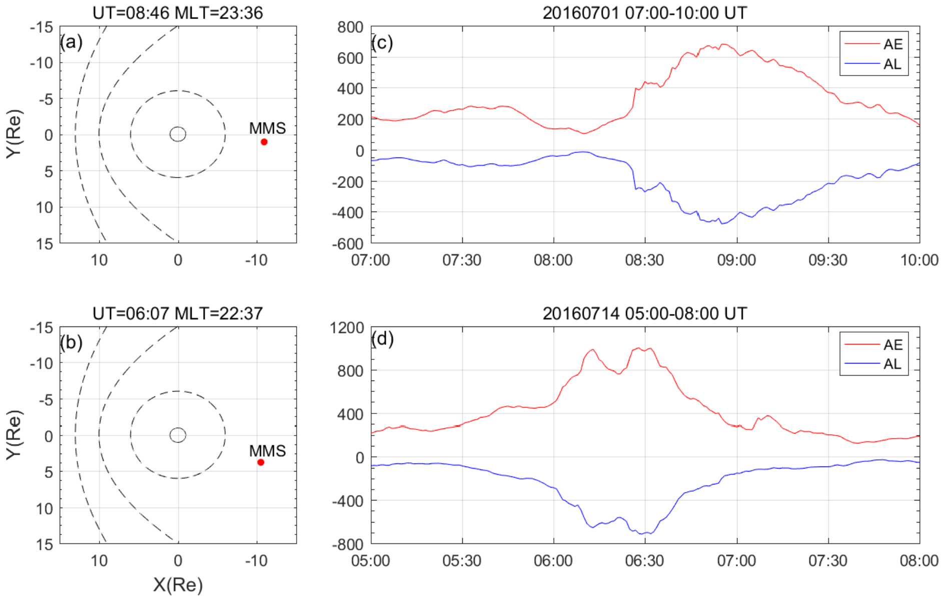

Figure 1.Locations of MMS at (a) 01 July 2017 08:46 UT and (b) 14 July 2016 06:07 UT in the X–Y plane, variations of AE index (red line) and AL index (blue line) from (c) 07:00 to 10:00 UT on 01 July 2016 and (d) 05:00 to 08:00 UT on 14 July 2016.

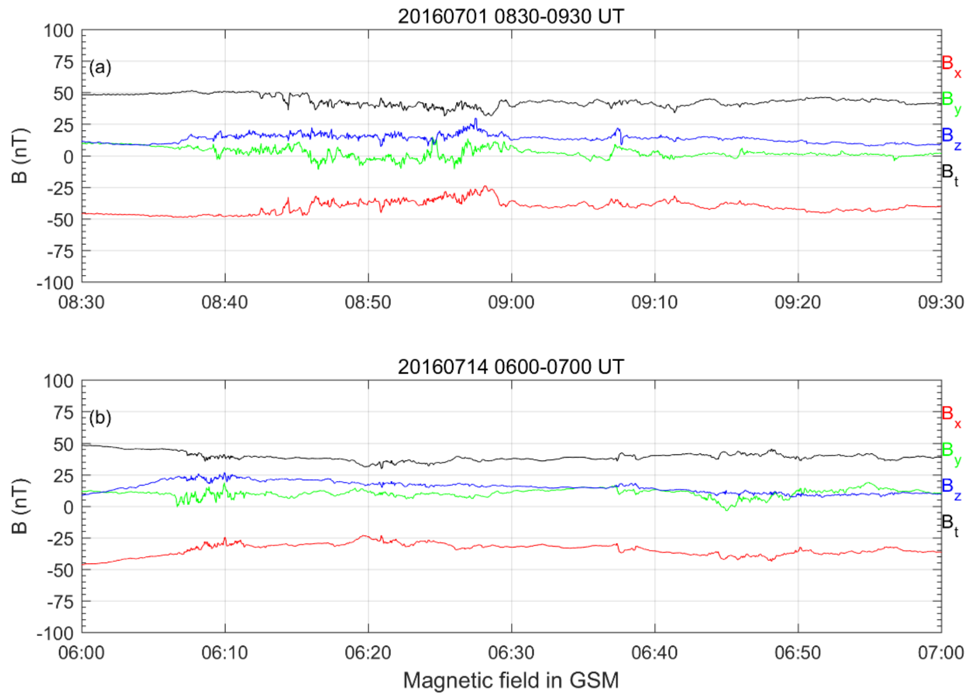

Figure 2.Overview of the magnetic field observed by MMS1 from (a) 08:30 to 09:00 UT on 01 July 2016 and (b) 06:00 to 07:00 UT on 14 July 2016. The red, green, blue, and black lines in the figure represent B_x, B_y, B_z and total magnetic field.

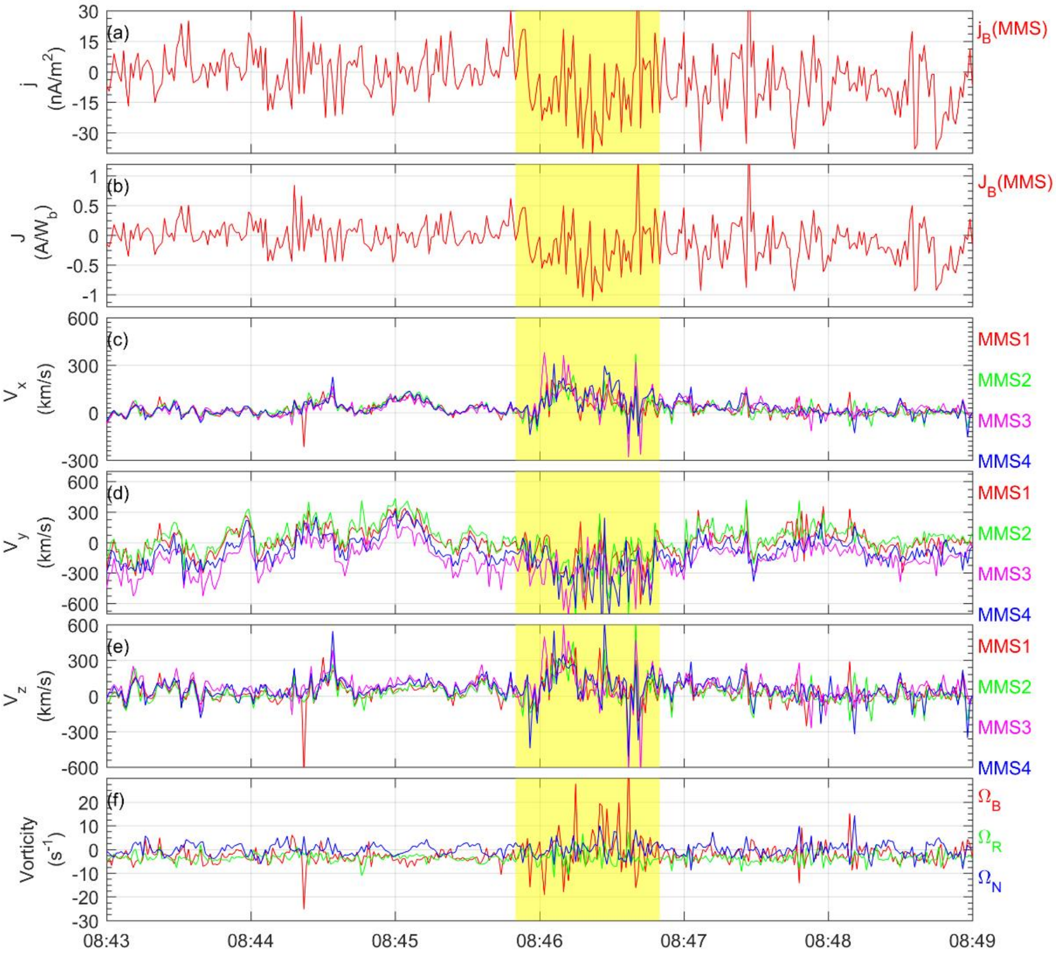

Figure 3.The substorm event on 1 July 2016, (a) the field-aligned componentof current density at the center of MMS in the local natural coordinates, (b) unit magnetic flux in magnetotail FACs at the center in MMS in the local coordinate system, drift velocity ((c) V_x, (d) V_y, and (e) V_z) in the GSM coordinate system, (f)vorticity at the center of MMS in the local natural coordinates. The shaded region represents the time corresponding to Earthwardplasma flow.

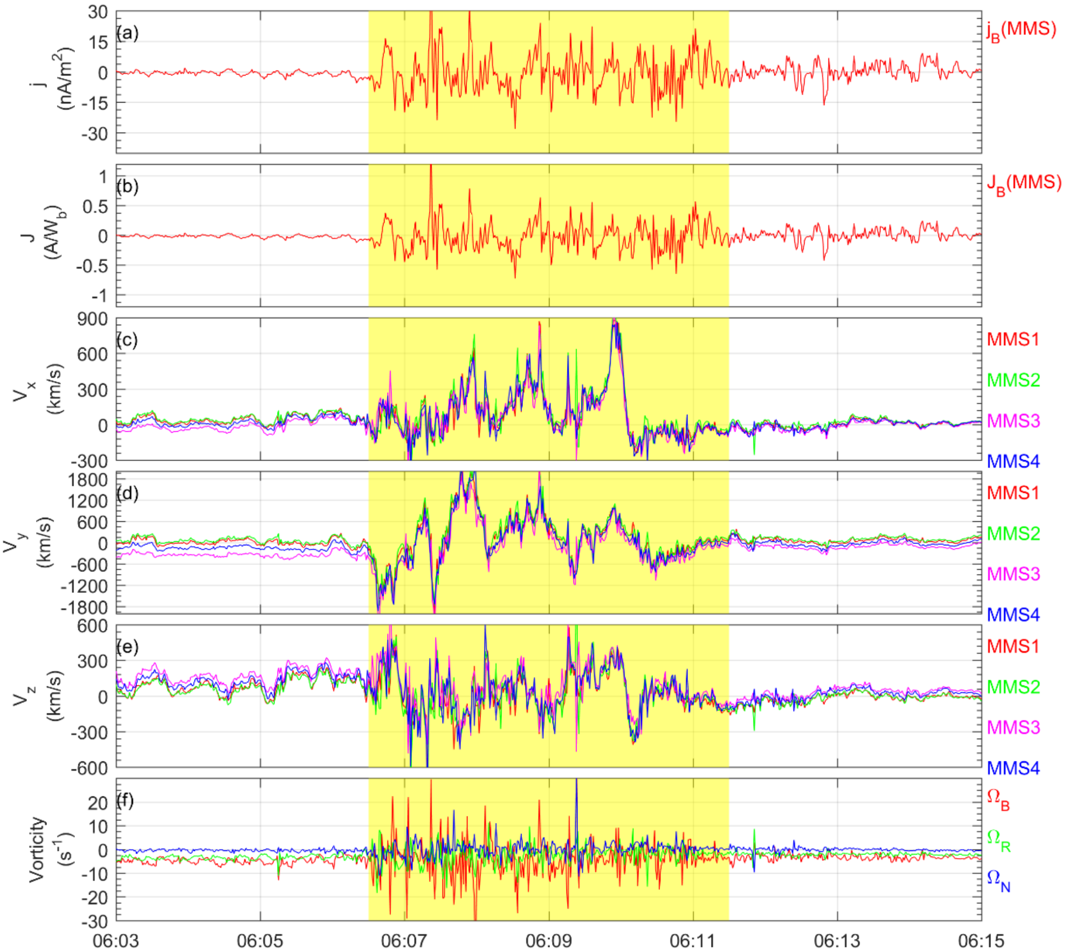

Figure 4.Overview of 14 July 2016 substorm in the same format as in Figure 3.

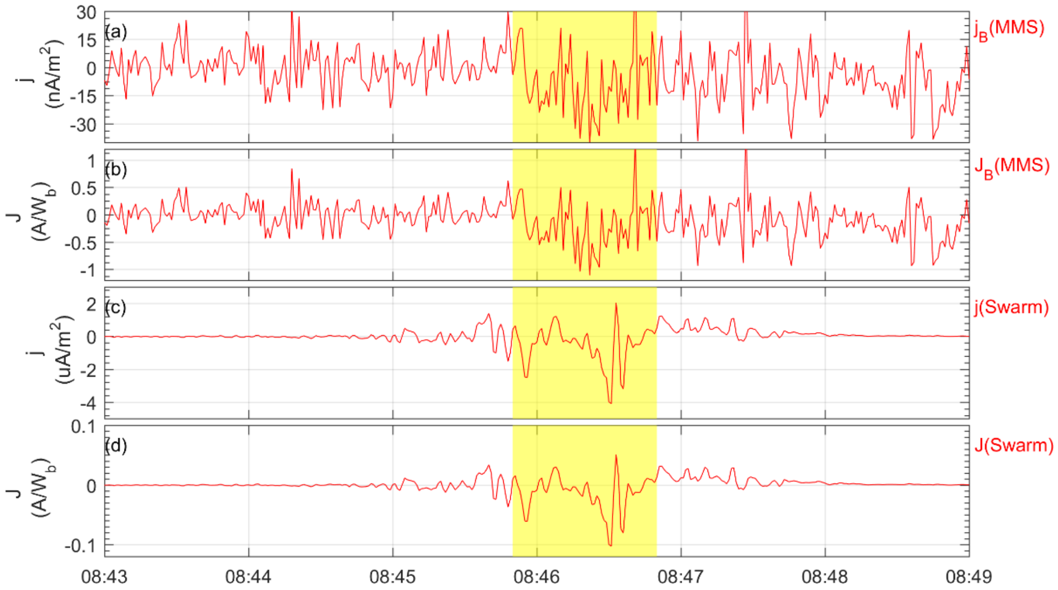

Figure 5.FACs observed by satellites for case 1, (a) the magnetotail current density, (b) the magnetotail FACs in unit magnetic flux, (c) the R1 type current density, (d) the R1 type FACs in unit magnetic flux.